Solution Structure of the PDZ2 Domain from Human Phosphatase hPTP1E and Its Interactions with C-Terminal Peptides from the Fas Receptor[†,‡]

Guennadi Kozlov and Kalle Gehring

Department of Biochemistry and Montreal Joint Center for Structural Biology, McIntyre Medical Science Building, McGill University, 3655 Drummond Street, Montreal, Quebec, H3G 1Y6, Canada

Irena Ekiel*

NMR Group, Pharmaceutical Biotechnology Sector and Montreal Joint Center for Structural Biology, Biotechnology Research Institute, National Research Council of Canada, 6100 Royalmount Avenue, Montreal, Quebec, H4P 2R2, Canada

Received August 16, 1999; Revised Manuscript Received September 21, 1999

ABSTRACT: The solution structure of the second PDZ domain (PDZ2) from human phosphatase hPTP1E has been determined using 2D and 3D heteronuclear NMR experiments. The binding of peptides derived from the C-terminus of the Fas receptor to PDZ2 was studied via changes in backbone peptide and protein resonances. The structure is based on a total of 1387 nonredundant experimental NMR restraints including 1261 interproton distance restraints, 45 backbone hydrogen bonds, and 81 torsion angle restraints. Analysis of 30 lowest-energy structures resulted in rmsd values of 0.41 ± 0.09 Å for backbone atoms (N, Cα, C′) and 1.08 ± 0.10 Å for all heavy atoms, excluding the disordered N- and C-termini. The hPTP1E PDZ2 structure is similar to known PDZ domain structures but contains two unique structural features. In the peptide binding domain, the first glycine of the GLGF motif is replaced by a serine. This serine appears to replace a bound water observed in PDZ crystal structures that hydrogen bonds to the bound peptide's C-terminus. The hPTP1E PDZ2 structure also contains an unusually large loop following strand β2 and proximal to the peptide binding site. This well-ordered loop folds back against the PDZ domain and contains several residues that undergo large amide chemical shift changes upon peptide binding. Direct observation of peptide resonances demonstrates that as many as six Fas peptide residues interact with the PDZ2 domain.

PDZ domains belong to a group of modules mediating interactions between proteins (*1*−*3*). Hundreds PDZ domains are known (*1, 4*−*9*). They are associated with receptors, membrane channels, and signal transduction proteins and are involved in spatial localization and clustering into functional complexes of proteins and in targeting signaling molecules to the plasma membrane. There is ample evidence for binding of PDZ domains to C-terminal peptides of target proteins (*4, 5, 10, 11*). For the majority of PDZ domains, a consensus sequence of three C-terminal amino acids, (Thr/Ser)-x-Val, is critical for binding. However, a growing number of the PDZ domains are known with alternative consensus sequences that include Ile or Leu at the C-terminus and Tyr, Phe, or Asp in the −2 position (*3, 12*−*14*) as well as internal peptide sequences (*15*−*20*).

The cytosolic human phosphatase hPTP1E (*21*−*23*), also known as PTPL1, PTP-BAS, or FAP-1, contains five PDZ domains. hPTP1E includes a band 4.1 homology region and most likely participates in a multiprotein complex at the plasma membrane−cytoskeleton junction. Multiple binding partners have been identified for hPTP1E; many of them are receptors or other membrane-associated proteins. These binding proteins include Fas (*10*), ephrin (*24*), transcription factor inhibitory protein IκBα (*25*), lim domain proteins ZRP-1 (*14*), RIL (*19*), and phosphatase-associated RhoGAP (*6*). The interactions between hPTP1E and the Fas receptor are mediated primarily by the second PDZ domain of hPTP1E, which was shown to act as a negative regulator of Fas-mediated apoptosis (*10*). This domain (residues 1361−1456) will be referred to as PDZ2 in this paper. The C-terminal fifteen amino acid fragment of Fas matches the PDZ binding consensus sequence and is critical for the hPTP1E−Fas interaction (*10*). More recently, it was shown that the C-terminal tripeptide (Ser-Leu-Val) of human Fas is necessary and sufficient for binding to PDZ2 and that this peptide can promote Fas-mediated apoptosis (*26*). PDZ4 domain from hPTP1E was also found to bind this peptide with high affinity (*27*).

Among currently known PDZ structures, there are complexes with C-terminal peptides (*11, 28*−*30*), internal peptides (*16*), and one unliganded structure (*31*). Interleukin-16 adopts a PDZ-like fold but does not bind peptides (*32*). The structures of the PDZ domains are very similar and consist of a β-sandwich of six strands and two α-helices. The C-terminal peptides are bound through their C-terminus in an extended binding groove capped by a characteristic carboxylate binding loop. By hydrogen bonding with the

[†] This study was supported by a grant from the Medical Research Council of Canada to K.G.

[‡] PDB accession number: 3PDZ.

* To whom correspondence should be addressed. Fax: (514) 496-5143. E-mail: Irena.Ekiel@bri.nrc.ca.

10.1021/bi991913c CCC: $19.00
Published on Web 02/16/2000

second β-strand of the PDZ domain, the bound peptide forms an expanded β-sheet. The side chain of C-terminal peptide residue fills a hydrophobic pocket formed by the PDZ β-sandwich and one α-helix. The peptide carboxylate is bound by a network of hydrogen bonds formed by the highly conserved carboxylate binding loop (typically, Arg/Lys-x-x-x-Gly-Leu-Gly-Phe), which was the first feature recognized in PDZ domains (*33*).

X-ray and solution structures for peptide−PDZ complexes show between four and five peptide residues interacting with PDZ domains. Specificity seems to be strongest for peptide residues 0 and −2, counting from the C-terminus. In the complex between the third PDZ domain from PSD95 and a bound peptide, temperature factors for peptide atoms are lowest at the C-terminus and increase 3-fold at residue −4 (*11*). Similarly, the solution structure of α-syntrophin complex indicates that five C-terminal peptide residues bind to the PDZ domain although with a much expanded peptide specificity (*28*). The PDZ domain from hCASK demonstrates a very different binding specificity as compared to PDZ2, but the major specificity determinants are the three C-terminal residues (*29*). Recent advances in engineering PDZ domains demonstrated novel recognition properties (*34*). Using artifical PDZ domains selected via a mutagenesis screen, these researchers used engineered PDZ domains to deliver target proteins to specific subcellular compartments.

Because of the biological relevance of PDZ2 in hPTP1E−Fas interactions and the general interest in understanding specificity differences between PDZ domains, we have determined the solution structure of the second PDZ domain from hPTP1E. In addition to presenting the PDZ2 structure, we provide the results of binding studies with 15- and 8-residue peptides from the C-terminus of the Fas receptor. These studies show that as many as six Fas residues interact with the PDZ2 domain and constitute an important step in a systematic structure-binding study of the second PDZ domain from the phosphatase hPTP1E.

MATERIALS AND METHODS

Production and Purification of the PDZ2 Domain. PDZ2 (1361−1456) from human phosphatase hPTP1E was expressed in *Escherichia coli*, either as a fusion protein with glutathione transferase (GST)[11] or using the pET expression system with pT7.7 promoter (Banville et al., unpublished results). ^{15}N-Enriched, ^{13}C-enriched, and ^{15}N/^{13}C-enriched PDZ2 domain was produced by growth of *E. coli* on a minimal medium containing ^{15}N-enriched ammonium sulfate and ^{13}C-enriched glucose as a source of nitrogen and carbon, respectively.

Protein purification was performed using ion exchange chromatography (Q-Sepharose Fast Flow from Pharmacia) followed by the size exclusion chromatography as described previously (*35*, *36*). The GST-PDZ2 fusion protein was purified using affinity chromatography on a glutathione sepharose column (Pharmacia). Protein purity and correctness of the sequence was verified electrophoretically by SDS−PAGE (using a Pharmacia Phast gel system) and mass spectrometry (API III MS/MS System, Sciex, Thornhill, ON, Canada). ^{15}N-Enriched ammonium sulfate and ^{13}C-enriched glucose were from Cambridge Isotope Laboratories, Andover, MA. All other chemicals were from Sigma and used without further purification.

Peptide Synthesis. Peptides were synthesized on a 396 Multiple Peptide Synthesizer (Advanced ChemTech, Louisville, KY) using conventional Fmoc solid-phase peptide synthesis, as described before (*35*, *36*). The peptides were purified by HPLC (Vydac C4 preparative column, 4.6 × 25 cm), using a linear gradient of 20−50% acetonitrile in 0.1% TFA. Purity was evaluated by an analytical run on a Vydac C18 column and was 98% or higher. The final products were lyophilized and identified using SCIEX API II mass spectrometer (Sciex, Thornhill, ON, Canada).

NMR Spectroscopy. PDZ2 samples for NMR experiments were 1.0−5.0 mM in 50 mM sodium phosphate buffer and 0.15 M NaCl at pH 6.8 at 293 K. This pH was selected so that His71, which is important for peptide binding, would be in the "physiological" nonprotonated state. For experiments on peptide binding to the GST-PDZ2 fusion protein, the pH of the phosphate buffer was lowered to 6.0 as higher pH values caused significant broadening of the peptide amide resonances due to solvent exchange. The NMR experiments were carried out on a Bruker DRX500 spectrometer equipped with an actively shielded *x*-,*y*-,*z*-axis gradient, triple resonance probe, and Bruker pulse field gradient accessory. Chemical shifts were measured relative to internal DSS for ^{1}H and calculated assuming $\gamma_N/\gamma_H = 0.101329118$ and $\gamma_C/\gamma_H = 0.251449530$ for ^{15}N and ^{13}C, respectively (*37*). NMR spectra were processed using GIFA (*38*) and XWINNMR Bruker software using Silicon Graphics computers. Peak tabulation and integration were performed using XEASY (*39*).

Self-Diffusion Measurements and Peptide-Binding Studies. Pulse field gradient NMR self-diffusion measurements were carried out using the stimulated echo technique (*40*, *41*). The *z*-axis gradient coil was used to generate the encode/decode gradients. The experiments were performed using 1.5 mM PDZ2 domain as described previously (*42*). Gradient strengths were calibrated using a sample of 0.1% $^{1}H_2O$ in $^{2}H_2O$ and literature values for $^{1}HO^{2}H$ diffusion coefficients (Longsworth, 1960). Protein signal decays were measured as a function of gradient strength at five different proton frequencies, and the results were analyzed using nonlinear regression.

The interactions of peptides with a GST-PDZ2 fusion protein were studied at constant 2 mM peptide concentrations and various protein:peptide molar ratios of up to 1:10. NMR signal assignments for the free peptides were performed using TOCSY and NOESY spectra. These assignments could be used for the complexes with the fusion protein as the peptides were always in large excess and in fast exchange.

Structure Calculations. Structures were calculated using the simulated annealing protocol implemented in the program CNS (version 0.3) (*43*). NOE restraints were obtained from ^{15}N- and ^{13}C-separated 3D NOESY experiments using mixing times of 35, 50, and 150 ms and from a 2D NOESY spectrum (110 ms mixing time) of unlabeled PDZ2. Distance constraints were classified according to the peak intensities as strong (1.8−3.0 Å), medium (1.8−4.0 Å), and weak (1.8−5.0 Å). The ϕ torsion angles were derived from an

[1] Abbreviations: NMR, nuclear magnetic resonance; GST, glutathione S-transferase; NOE, nuclear Overhauser effect; NOESY, nuclear Overhauser enhancement spectroscopy; TOCSY, total correlated spectroscopy; HSQC, heteronuclear single-quantum coherence spectroscopy; SA, simulated annealing; PFG, pulse field gradient.

Table 1: Structure Statistics of the PDZ2 Domain from Human Phosphatase hPTP1E

restraints for structure calculations	
total restraints used	1387
total NOE restraints	1261
intraresidue	348
sequential ($\|i - j\| = 1$)	321
medium range ($1 < \|i - j\| \leq 4$)	135
long range ($\|i - j\| > 4$)	457
hydrogen bonds restraints	45
dihedral angles restraints	81
statistics for structure calculations	⟨SA⟩[a]
rmsd from idealized covalent geometry	
bonds (Å)	0.0024 ± 0.0001
bond angles (°)	0.46 ± 0.01
improper torsions (°)	0.37 ± 0.01
rmsd from experimental restraints[b]	
distances (Å)	0.017 ± 0.01
final energies (kcal mol^{-1})	
E_{total}	233.5 ± 3.4
E_{bonds}	8.5 ± 0.3
$E_{impropers}$	14.9 ± 1.2
E_{vdw}[c]	89.5 ± 4.0
E_{NOE}	32.6 ± 1.8
coordinate precision[d] (Å)	⟨SA⟩ versus $\overline{\langle SA \rangle}$
rmsd of backbone atoms (N, Cα, C′) for residues 4−92	0.41 ± 0.09
rmsd of all heavy atoms for residues 4−92	1.08 ± 0.10
comparison of PDZ2 hPTP1E vs syntrophin PDZ structures (Å)	
rmsd Cα atoms for secondary structure elements	1.33
rmsd Cα atoms for β2, β3 and α2	1.18
Ramachandran plot statistics[e] (%)	
residues in most favored regions	74.4
residues in additional allowed regions	24.4
residues in generously allowed regions	1.3

[a] ⟨SA⟩ refers to the ensemble of the 30 structures with lowest energy from 200 calculated structures. [b] No distance restraint in any of the structures included in the ensemble was violated by more than 0.3 Å. [c] Repel = 0.8 for the final step of calculations. [d] rmsd between the ensemble of structures ⟨SA⟩ and the average structure of the ensemble $\overline{\langle SA \rangle}$. [e] Generated using PROCHECK on the average minimized structure.

HNHA experiment (*44*). The statistics for the structure calculations are shown in Table 1.

RESULTS AND DISCUSSION

Resonance Assignments for PDZ2. Figure 1 shows the ^{1}H−^{15}N HSQC spectrum of the uniformly ^{15}N-enriched PDZ2 domain from hPTP1E, demonstrating good signal dispersion characteristic of a folded, β-sheet-rich protein. Backbone NMR signal assignments were previously determined using doubly ^{13}C/^{15}N-enriched protein and heteronuclear HNCA, HN(CO)CA, HNCACB, and CBCA(CO)NH experiments (*36*). Additional HNCO, HN(CA)HA, and HBHA(CO)NH experiments were used to resolve problems of signal overlap and carbon chemical shift ambiguities.

Side chain signal assignments were performed using H(C)CH−COSY, (H)CCH−COSY experiments (*45*), ^{13}C-resolved TOCSY (*46, 47*), ^{13}C-NOESY−HMQC, and ^{13}C-TOCSY−HMQC (*48*) experiments. Stereospecific assignments for 22 of 53 prochiral β methylene protons were obtained using HAHB (*49*), HN(CO)HB (*50*). and HNHB (*51*) experiments. Ten percent ^{13}C-labeled protein (*52*) was used to obtain stereospecific assignments for 32 of 40 valine and leucine isopropyl methyl groups present in the PDZ domain. Additional 3D ^{15}N-NOESY−HMQC and ^{15}N-TOCSY−HMQC experiments were used for assignment of ^{1}H/^{15}N signals in the PDZ2/peptide complex.

There are four arginine residues in the domain. Their ϵ protons were assigned using a 2D ^{15}N-TOCSY−HMQC experiment. The ϵ proton of Arg51 is strongly shifted downfield because it is located in the plane of the aromatic ring of Phe7. Interestingly, the ϵ proton of Arg79 at the top of second helix shifts upon peptide binding. This observation suggests that the side chain of Arg79 participates in peptide binding.

Structure. The overall fold of PDZ2 is similar to previously determined PDZ domain structures (*11, 28*−*32*). The structure comprises six β-strands and two α-helices (Figure 2A,B). The β-strands form a β-sandwich with β1 (Ile6-Leu11), β6 (Val85-Glu90), β4 (Arg57-Val61), and β5 (Val64-Ser65) participating in one β-sheet and strands β2 (Ile20-Thr23), β3 (Ile35-Val40), and β4 forming a second β-sheet. The planes of these β-sheets are not parallel, which allows β4 to participate in both sheets. All β-strands in the sheets have an antiparallel orientation. α-Helices are formed by Ala45-Asp49 (α1) and His71-Arg79 (α2). Hydrophobic residues Ile20, Val22, Val58, Val61, Val75, Leu78, and Leu87 form the core of the PDZ domain. The backbone hydrogen bonds present in the final structures are generally in agreement with previously reported amide exchange rates (*35*). Most of the hydrogen bonds are located within secondary structure elements. Outside these regions, amide of Lys13 formed a hydrogen bond with carbonyl of Gln83 and Ile41 with Gly19, Asn62 with His86, and Leu66 with Leu59. The amide of His53 was found to hydrogen bond with the side chain of Asp56.

The N- and C-termini are disordered in the structure and were not used in rmsd calculations. On the other hand, the carboxylate-binding loop and the loop between β2 and β3

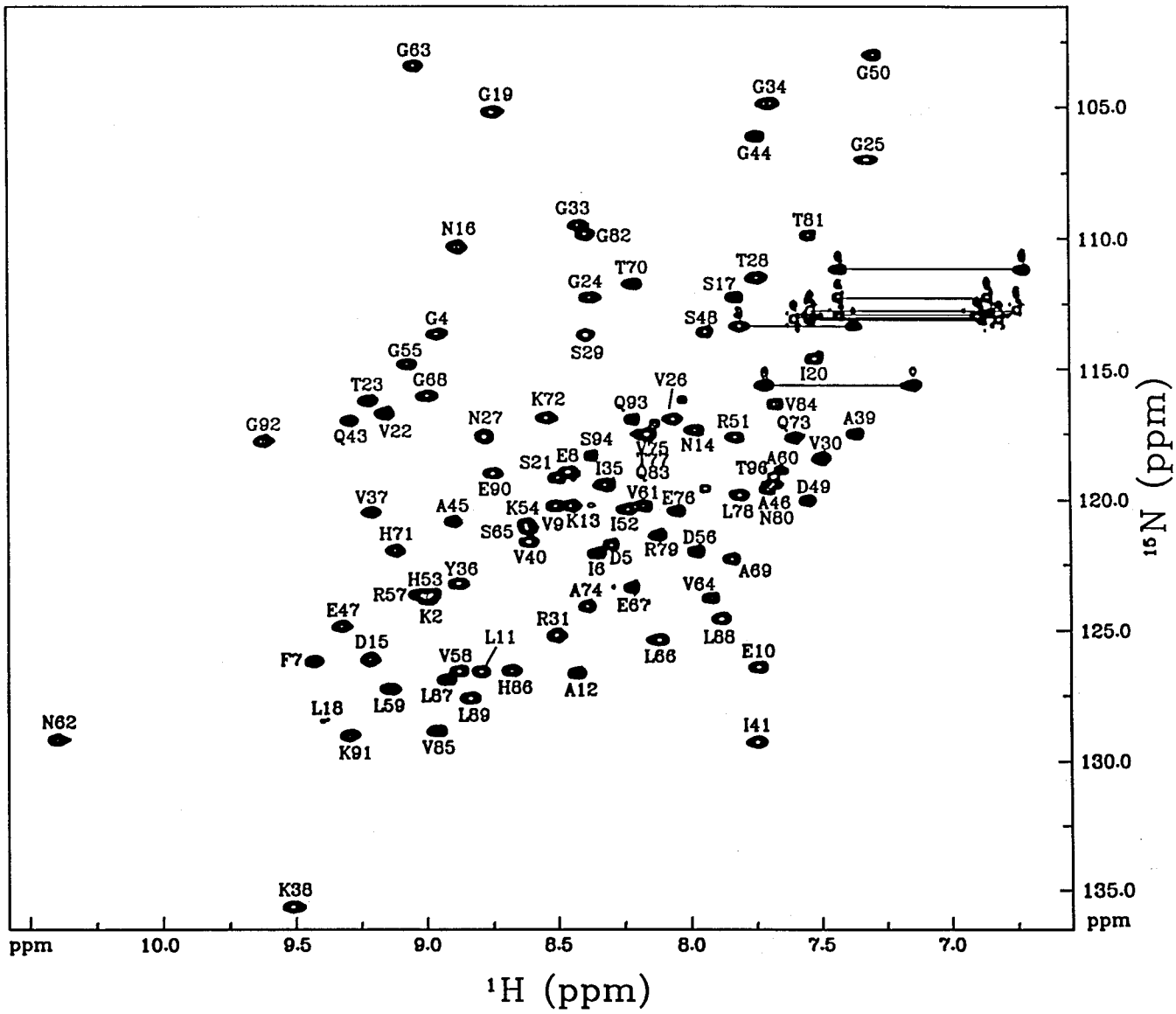

FIGURE 1: 2D ^{1}H−^{15}N HSQC spectrum of ^{15}N-enriched PDZ2 domain from human phosphatase hPTP1E. The spectrum was acquired at 293 K in 50 mM phosphate buffer (pH 6.8) and 0.15 M NaCl at a protein concentration of 2 mM.

strands are more structured than in previously determined PDZ structures. Even the long loop Gly25-Gly33 is only slightly more disordered than the secondary structure elements. Analysis of NMR relaxation measurements showed high (>0.7) generalized order parameters for nearly the whole domain (data not shown).

The general fold of PDZ domains is known from the early work on the third PDZ from the synaptic protein PSD-95 (*11*) and the third PDZ domain of the human homologue of the *Drosophila* tumor suppressor gene product, *Dlg*A (*31*). Two important differences between the PDZ2 domain from hPTP1E and previously studied PDZ domains are the replacement of the first glycine in the GLGF motif by Ser17 and the longer loop (Gly25-Gly33) following strand β2.

The GLGF motif was the first sequence motif identified in PDZ domains (*33*). In PDZ2, the GLGF motif is replaced by the sequence SLGI. These residues occur at the top of the peptide binding cleft before strand β2 and participate in hydrogen bonding with the C-terminal carboxyl group of bound peptides through the amides of the last three residues (*11*, *29*). Ser or Thr occurs in the first position of the GLGF motif in roughly 20% of the PDZ sequences listed in the ProDom database (*53*). The side chains of both the second and fourth amino acids in the GLGF motif are pointed toward the protein interior and are invariantly hydrophobic. Structures of PDZ domains containing both Ile or Phe at position 4 have been determined. The structure of the binding site was not altered by this replacement.

In crystal structures of PDZ−peptide complexes, there are three hydrogen bonds between the peptide carboxylate and protein amides while a fourth hydrogen bond is made by a bound water molecule. This water is held in place by the side chain of the conserved lysine or arginine that precedes the GLGF motif (i.e., Lys13 in our structure). In PDZ2, this water molecule appears to be replaced by the hydroxyl of Ser17 (Figure 2C). The stereospecific assignment of methylene protons of this residue was done to ensure the position of the serine side chain in the structure. In 75% of the calculated NMR structures, the distance between the side chain nitrogen atom of Lys13 and side chain oxygen atom of Ser17 is less than 4 Å. No electrostatic force field was used to calculate the structures. Thus, the side chain of Lys13

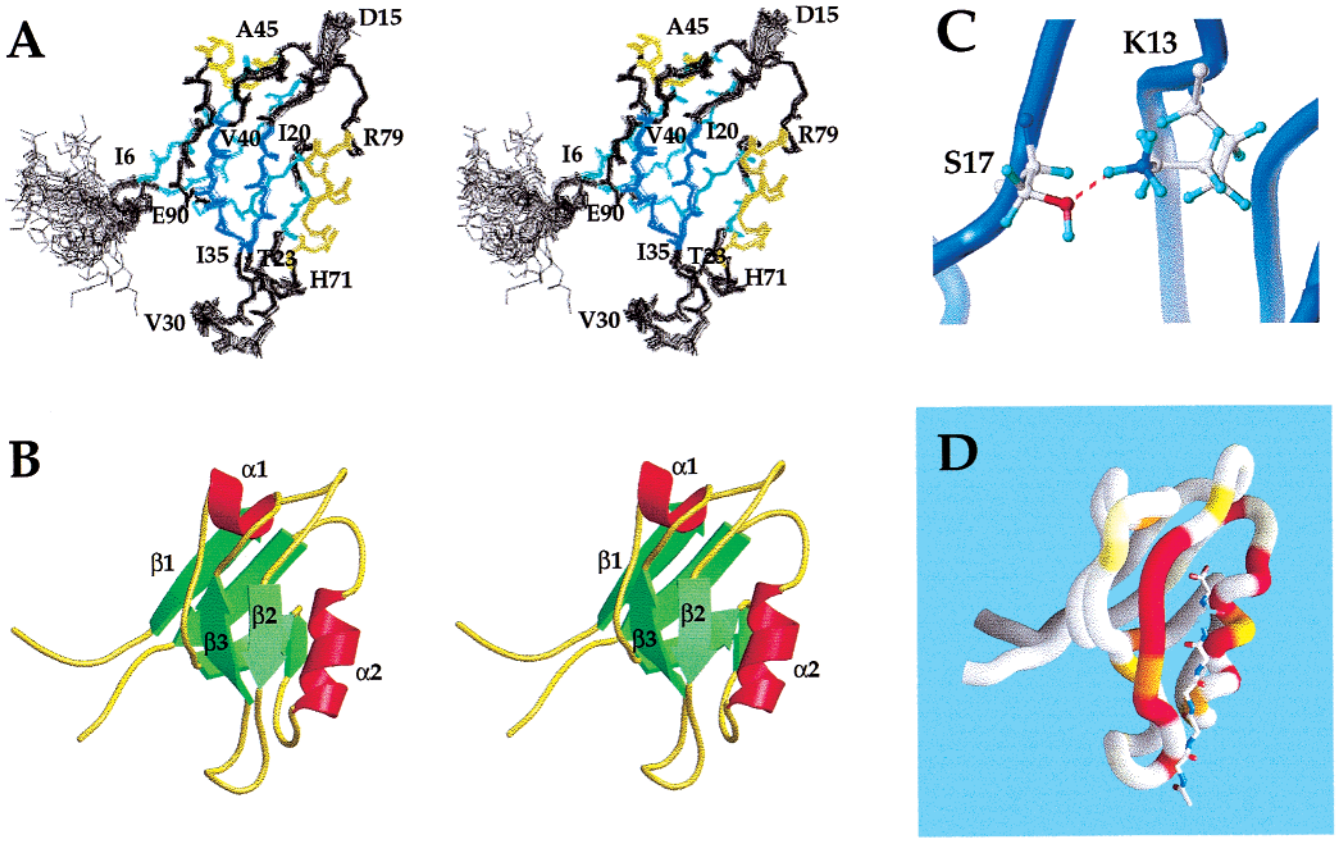

FIGURE 2: (A) Backbone overlay of the 30 lowest energy NMR structures of PDZ2 domain from human phosphatase hPTP1E. β-Sheets β1-β6-β4-β5 are colored cyan, β-sheets β2-β3 are blue, and α-helical residues are yellow. (B) Ribbon representation of the average PDZ2 structure generated with MOLSCRIPT (*55*). (C) One of the PDZ2 structures showing the hydrogen bond between the side chains of Ser17 and Lys13. The hydroxyl of Ser17 is poised to donate a hydrogen bond to the C-terminus of an incoming peptide. (D) Representation of a complex of PDZ2 with the six C-terminal residues of the Fas receptor generated with GRASP (*56*). The backbone trace of PDZ2 is color-coded according to the size of the chemical shift change upon peptide binding. Residues uninfluenced by peptide binding are shown in white; residues with ^{1}H plus ^{15}N chemical shift differences of ~0.75 ppm are yellow, ~0.9 ppm are orange, and above 1 ppm are red. The peptide backbone was modeled in an extended conformation and docked into the domain to accommodate the chemical shift changes. The peptide was not included in structure calculations, and no special docking program, algorithm, or procedure was used in the placement of the peptide.

appears to make a hydrogen bond with the side chain oxygen of Ser17. This conclusion is supported by observation of unusually slow-exchanging NH_3 protons of two lysines, Lys13 and Lys72. Their chemical shifts are different from the random coil values (7.13 vs 7.52 ppm, respectively). Since these peaks are broad, no NOE cross-peaks were found for them. Their slow exchange is likely due to hydrogen bonding with the side chains of Ser17 and Glu76, respectively. In PDZ2−peptide complexes, this would position the hydroxyl hydrogen of Ser17 to make a fourth hydrogen bond with the peptide C-terminus. Future structural work on PDZ2−peptides complexes should test this model.

The loop between strands β2 and β3 is enlarged in PDZ2 and includes an extra 3−5 amino acids relative to known PDZ structures. The loop folds toward the protein core positioning the isopropyl group of Val30 into a small hydrophobic pocket. In previously studied PDZ−peptide complexes, this loop was generally not considered to influence ligand binding. In PDZ2, the long structured loop may provide an additional site for the peptide binding and increase the selectivity of the PDZ domain for the recognition of its natural partners. This loop is the site of an alternative splicing in hPTP1E (*21*). In the longer variant of hPTP1E, this loop is further extended and includes the sequence Val-Leu-Phe-Asp-Lys between Thr23 and Gly24. This would likely change the conformation of this loop and affect the selection of binding partner(s).

^{1}H−^{15}N HSQC Spectra of the PDZ2 Domain in Complex with Fas-Derived Peptides. Two different approaches were taken to characterize binding of the Fas C-terminal peptides to the PDZ2 domain. The first consisted of monitoring exchange-induced line broadening of peptide resonances and the second consisted of comparing PDZ resonances in ^{15}N-labeled protein with and without a peptide. Two peptides derived from the C-terminus of the Fas receptor were used to study interactions with PDZ2. The first peptide contained 15 amino acids, Asp-Ser-Glu-Asn-Ser-Asn-Phe-Arg-Asn-Glu-Ile-Gln-Ser-Leu-Val, and the second was truncated to the eight C-terminal residues, Arg-Asn-Glu-Ile-Gln-Ser-Leu-Val. We estimate the binding constant for the latter peptide to be roughly 30 μM ± 35% (*35*). Titration of the PDZ2 domain with either of the peptides led to intermediate exchange spectra in which the PDZ2 amide signals were extensively broadened at sub-stoichiometric peptide concentrations (results not shown). Titrations were extended to a 30% molar excess of the peptide over protein that was sufficient to obtain narrow lines in the spectra of the complexes. For signal assignments in the complex, a 3D NOESY−HMQC experiment was performed, and the spectrum was compared with that for the free PDZ2 domain. The

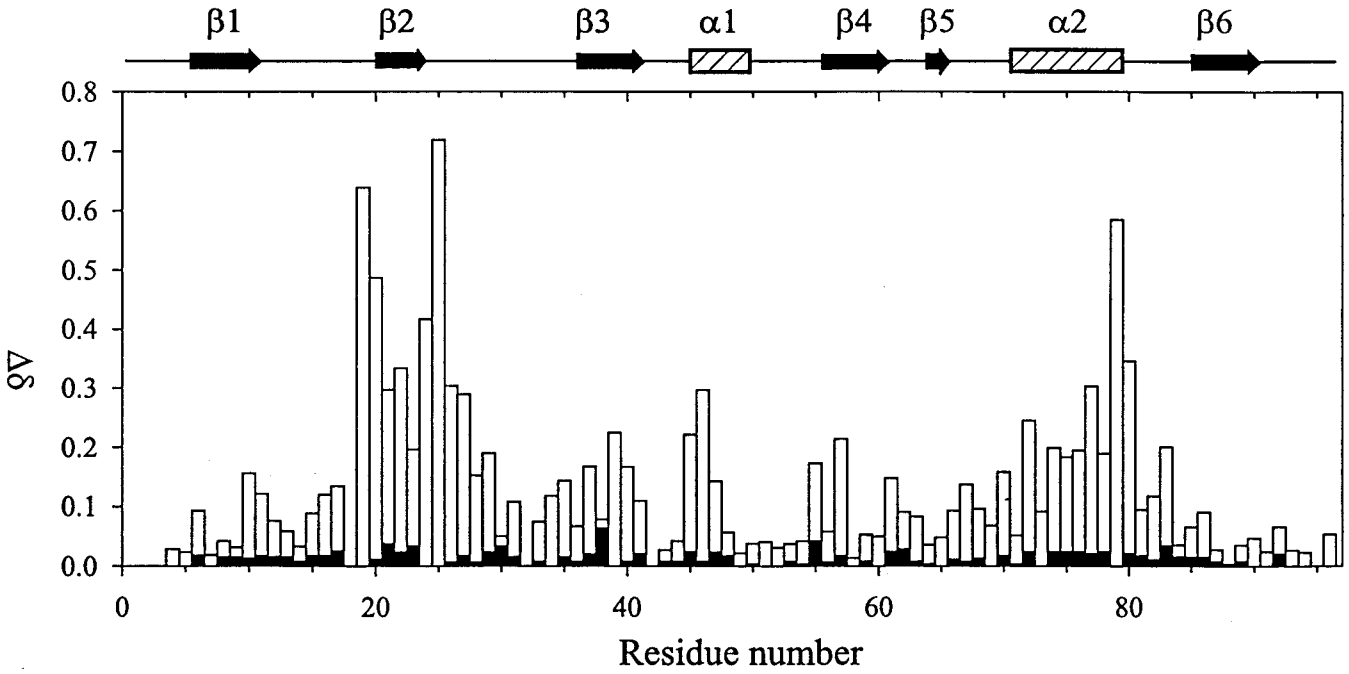

FIGURE 3: Histogram showing differences in amide chemical shifts in the free PDZ2 domain and its complex with C-terminal peptides from the Fas receptor. Open bars represent amide chemical shift differences between the free PDZ2 domain and its complex with the 8-residue Fas peptide calculated according to the formula $[(0.17\Delta N)^2 + (\Delta H)^2]^{1/2}$ (*57*). Solid bars show chemical shift differences between PDZ2 complexed with 15- and 8-residue Fas peptides. Secondary structure elements are shown schematically above the diagrams.

similarity of NOEs (both presence and intensities of cross-peaks) suggests a very similar overall fold for both ligand-free and liganded forms of the protein, as was observed for the third PDZ domain from PSD-95 (*11*).

Although the overall conformation of the protein did not change, the HSQC spectra showed significant chemical shift changes for many of the amide signals upon complex formation. Average chemical shift differences were 0.15 and 0.79 ppm in the proton and nitrogen dimensions, respectively. The amino acids experiencing the largest changes in chemical shift clustered in two regions: residues 19−27 and residues 70−79 (Figures 2D and 3). According to the obtained structure, the part of the carboxylate binding loop (residues 17−19), the second β-strand (residues 20−23), and the long α-helix (residues 71−79) are expected to be in direct contact with the peptide. Residues Gly19, Ile20, and Ser17 showed the largest changes. For Gly19 and Ile20, the large chemical shift change is most likely due to hydrogen bond formation during peptide binding. In the extended loop following strand β2, Asn27 showed a significant chemical shift change upon peptide binding. The results suggest that PDZ2 binds the peptides in a fashion similar to that observed for other PDZ domains but with a slightly extended binding site.

Amide chemical shifts for the PDZ2 complexes with the two different Fas peptides were compared. The differences in chemical shift changes between the two complexes were very small (below 0.02 and 0.2 ppm in the proton and nitrogen dimensions, respectively), and no clustering was observed in any particular region of the protein (Figure 3). Overall, the magnitude of chemical shift differences between the complexes was more than 10-fold smaller than changes induced upon complex formation itself. These results suggest that the first seven residues in the 15 residue peptide do not interact with PDZ2.

The participation of individual peptide residues in complex formation was studied using the fast exchange kinetics of PDZ2-Fas peptide binding. Because the small size of the PDZ2 domain alone (10 kDa) limits the broadening effects that could be observed, a larger GST-PDZ2 fusion protein was used in these binding experiments. Peptide was titrated with protein to give a final protein:peptide molar ratio of 1:10. High-resolution 1D and 2D TOCSY spectra were used to monitor the progressive broadening of peptide amide signals. This line broadening allowed us to identify residues immobilized in the peptide−protein complex. Figure 4 shows fragments of the TOCSY spectra for a peptide alone (panel A) and for a complex at a peptide:protein ratio of 10:1 (panel B). A comparison indicates broadening of amide signals for amino acids Glu10, Gln12, Ser13, Leu14, and Val15 and the side chain signals (but not amide resonance) of Ile11. These correspond to positions 0 to −5 when numbered from the peptide C-terminus. Very little broadening was observed for amide signals of remaining amino acids. On the basis of the NMR measurements, we conclude that the six C-terminal peptide residues are in contact with the protein.

Functional studies presented by Saras et al. (*27*) show that the last five amino acids of the Fas receptor contribute to binding to PDZ2. On the other hand, Yanagisawa et al. (*26*) conclude that the last three amino acids give full inhibition of the Fas−hPTP1E binding. Our structural studies provide a very different approach to the same issue, classifying interacting residues based on their NMR relaxation properties and chemical shifts. In this way, even weak interactions can be detected. Additionally, the structural approach taken in this work is free of artifacts occasionally arising from immobilization/linker effects in binding assays (*54*).

While the peptide C-terminal sequence (Ser/Thr)-x-Val is very important for binding in many PDZ domains, the preceding amino acids certainly determine both the binding affinity and specificity of PDZ domains (*6*, *12*, *28*). Further NMR studies, using peptides with higher affinity than the C-terminal peptide from Fas receptor, are in progress with

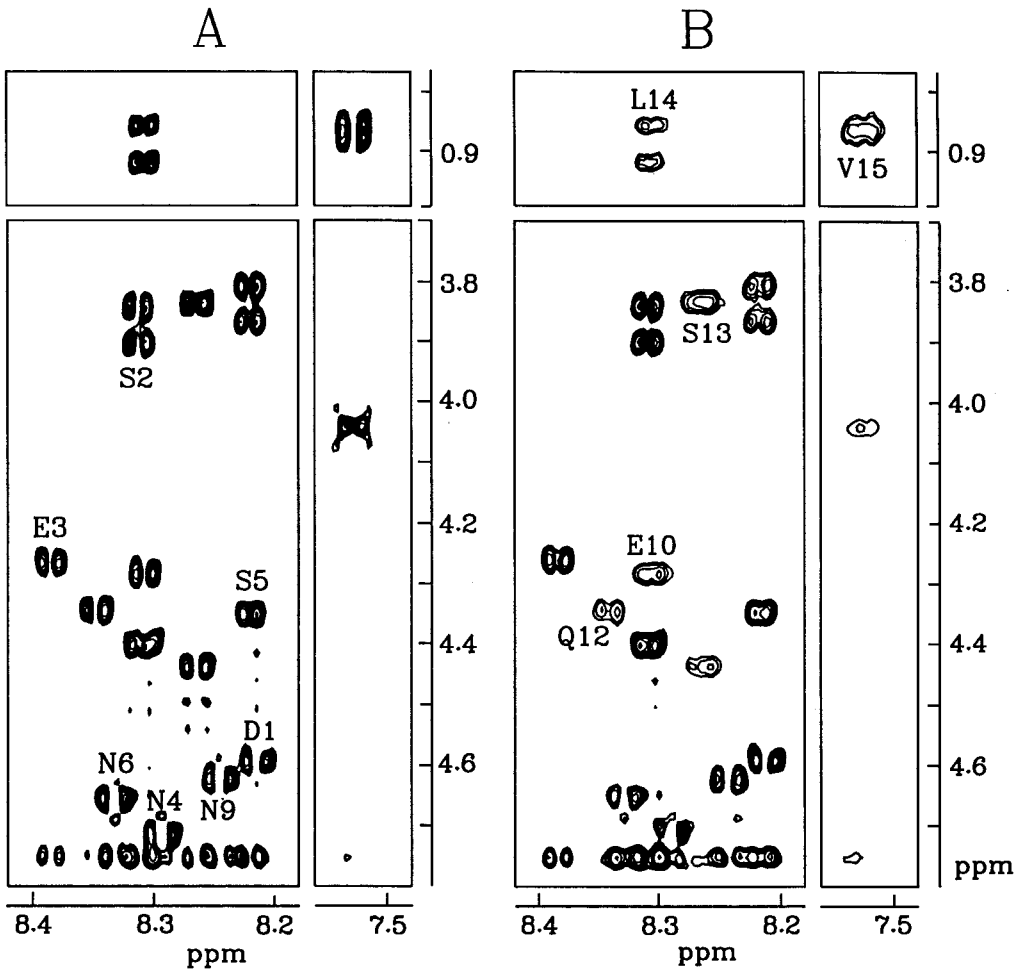

FIGURE 4: Fragments of 2D TOCSY spectra of (A) the free 15-amino acid C-terminal peptide from the Fas receptor. (B) The same peptide in a 10:1 complex with the GST-PDZ2 fusion protein. Noninteracting peptide residues are labeled in panel A. Interacting peptide residues with broadened amide resonances are labeled in panel B. Residues Phe7, Arg8, and Ile11 are not shown. The TOCSY mixing time was 130 ms.

```
                    bbbbbb          bbbb                  bbbbbbb    aaaaa
PDZ1          1 SPEREITLVNLKKDAKYGLGFQIIGG---EKMGRLDLGIFISSVAPGGPADLDGCLKPGD
PDZ2          1 PKPGDIFEVELAKNDN-SLGISVTGG---VNTSVRHGGIYVKAVIPQGAAESDGRIHKGD
PDZ3          1 VTEENTFEVKLFKNSS-GLGFSFSREDNLIPEQINASIVRVKKLFPGQPAAESGKIDVGD
PDZ4          1 FELEVELLITLIKSEKGSLGFTVTKG----NQRI---GCYVHDVI-QDPAKSDGRLKPGD
PDZ5          1 MLPHLLPDITLTCNKE-ELGFSLCGG---HDS--LYQVVYISDINPRSVAAIEGNLQLLD
consensus     1       . .. * ..    **......        .   ..... . .  .*   .*... .*

                   bbbbb bb       aaaaaaaaa       bbbbbb
PDZ1         58 RLISVNSVSLEGVSHHAAIEILQNAPEDVTLVISQP
PDZ2         57 RVLAVNGVSLEGATHKQAVETLRNTGQVVHLLLEKG
PDZ3         60 VILKVNGASLKGLSQQEVISALRGTAPEVFLLLCRP
PDZ4         53 RLIKVNDTDVTNMTHTDAVNLLRAASKTVRLVIGRV
PDZ5         55 VIHYVNGVSTQGMTLEEVNRALDMSLPSLVLKATRN
consensus    61 ... **.... .... ...   *. .    . *.. .
```

FIGURE 5: Sequence alignment of five PDZ domains from human phosphatase hPTP1E. Conserved residues are shaded.

the general goal of providing a structural understanding of the role of residues −3 to −5 in binding specificity.

Homology Analysis of PDZ Domains from hPTP1E. Based on the PDZ2 structure, the five different PDZ domains from hPTP1E can be analyzed to address the issue of binding specificity. Specific proteins have been identified that bind to PDZ1, PDZ2, and PDZ4 domains (*6*, *10*, *14*, *19*, *24*, *25*). PDZ2 and PDZ4 both bind the Fas receptor, and not surprisingly, they share the highest similarity (40.2% identity). PDZ5 is the least similar to PDZ2 (28.2%) and as described below contains important differences in several key positions. No protein binding partners are known for hPTP1E domains PDZ3 and PDZ5.

Figure 5 shows the sequence alignment of the five hPTP1E PDZ domains. All of the PDZ domains share a conserved carboxylate binding loop and a hydrophobic pocket for peptide binding, including (Val/Leu/Ile)58, Val61, Leu87, and Leu78. The loop after β2 represents the main difference between PDZ2 and PDZ4. In PDZ2, this loop (Gly25-Gly33) is longer and possibly is responsible for the higher affinity

of PDZ2 toward the Fas C-terminal peptides. An important similarity between PDZ2 and PDZ4 is Ile41, which likely makes a hydrophobic contact with Leu(−1) of the peptide. PDZ3 also has a large hydrophobic residue (Phe) in this position while PDZ5 contains asparagine, which might select for a long charged residue in the peptide. Other common features of PDZ2 and PDZ4 include Thr23 at the end of strand β2 (which is similar to serine in PDZ3) and a serine instead of glycine at the beginning of the GLGF motif.

PDZ3 and PDZ5 are unique in the absence of the conserved histidine (His71) that contributes to binding specificity for Ser/Thr(−2) of the peptide. This histidine is replaced by a glutamine and leucine in PDZ3 and PDZ5, respectively, which should lead to a different sequence selection (*12*). PDZ5 also has an unusual carboxylate binding loop with cysteine in place of Lys13 and EGLF in place of the GLGF motif. We speculate that these changes in PDZ5 decrease the affinity of this domain to C-terminal sequences. PDZ5 also does not have Arg79 as found in domains PDZ2−4. Generally, we expect that PDZ3 has binding specificity similar to PDZ2 and PDZ4 with minor modifications, while PDZ5 has completely different selection criteria.

PFG NMR Self-Diffusion Measurements. Numerous PDZ domains are capable of forming heterotypic (*15, 16, 18*) and homotypic dimers (*31*), and it has been suggested that these interactions might have a regulatory function (*2*). To investigate the possibility of the dimer formation by PDZ2, self-diffusion experiments were carried out using the PFG stimulated echo NMR technique (*40, 41*). The translational self-diffusion coefficient at 293 K for both the liganded and free PDZ2 domain was 1.06×10^{-6} cm^2/s. This value agrees well with the molecular weight for monomeric PDZ2 (10 kDa). The value is higher than that obtained (0.94×10^{-6} cm^2/s) in a control experiment with lysozyme (14 kDa) and is much higher than expected, 0.80×10^{-6} cm^2/s, for a dimeric form of the PDZ2 domain (20 kDa). Thus, the NMR measurements indicate no dimer formation under the experimental conditions used (pH 6.8, room temperature, 50 mM phosphate, 0.15 M NaCl). On the basis of line width analysis, we can also rule out dimerization over the pH range from 3 to 9 (data not shown).

Recent structural work on the nNOS-syntrophin PDZ domain complex (*16*) describes a novel mechanism for PDZ dimerization. In this structure, C-terminal extension of the nNOS PDZ domain, in the form of a β-finger, is critical for formation of the complex. However, this mechanism cannot explain the reported homodimerization of the third PDZ domain from Dlg (*31*) because of the absence of a β-finger. Instead, the C-terminal extension of the Dlg PDZ domain forms an α-helix. This suggests that multiple modes of dimerization can exist for PDZ domains. The lack of self-association for the PDZ2 domain from human phosphatase hPTP1E indicates that the homodimerization mode found for the third PDZ domain from Dlg does not apply to hPTP1E PDZ2. Our results do not exclude possibility of association via a β-finger mechanism in hPTP1E, as only a short variant of the PDZ2 domain was studied. In fact, secondary structure prediction shows that the sequence following PDZ2 has some propensity for β-strand formation and displays similarity to the consensus β-finger sequence proposed by Hillier et al. (*16*). Identification of internal protein fragments capable of binding to PDZ domains constitutes a new challenge in understanding interactions of this important class of protein modules.

ACKNOWLEDGMENT

The authors thank Drs. Traian Sulea and Hervé Hogues for help with the structure calculations. We also acknowledge Drs. Dennis Banville and Shi H. Shen for the gift of plasmid-containing PDZ2. This is NRC Publication No. 42927.

SUPPORTING INFORMATION AVAILABLE

A table containing ^{1}H, ^{15}N, and ^{13}C chemical shift assignments for PDZ2 at pH 6.8, 293 K (5 pages). This material is available free of charge via the Internet at http://pubs.acs.org.

REFERENCES

1. Fanning, A. S., and Anderson, J. M. (1998) *Curr. Top. Microbiol. Immunol. 228*, 209−233.
2. Ponting, C. P., Phillips, C., Davies, K. E., and Blake, D. J. (1997) *Bioessays 19*, 469−479.
3. Saras, J., and Heldin, C. H. (1996) *Trends Biochem. Sci. 21*, 455−458.
4. Kornau, H. C., Schenker, L. T., Kennedy, M. B., and Seeburg, P. H. (1995) *Science 269*, 1737−1740.
5. Kim, E., Niethammer, M., Rothschild, A., Jan, Y. N., and Sheng, M. (1995) *Nature 378*, 85−88.
6. Saras, J., Franzen, P., Aspenstrom, P., Hellman, U., Gonez, L. J., and Heldin, C. H. (1997) *J. Biol. Chem. 272*, 24333−24338.
7. Shieh, B. H., and Zhu, M. Y. (1996) *Neuron 16*, 991−998.
8. Simske, J. S., Kaech, S. M., Harp, S. A., and Kim, S. K. (1996) *Cell 85*, 195−204.
9. Hemming, N. J., Anstee, D. J., Staricoff, M. A., Tanner, M. J., and Mohandas, N. (1995) *J. Biol. Chem. 270*, 5360−5366.
10. Sato, T., Irie, S., Kitada, S., and Reed, J. C. (1995) *Science 268*, 411−415.
11. Doyle, D. A., Lee, A., Lewis, J., Kim, E., Sheng, M., and MacKinnon, R. (1996) *Cell 85*, 1067−1076.
12. Songyang, Z., Fanning, A. S., Fu, C., Xu, J., Marfatia, S. M., Chishti, A. H., Crompton, A., Chan, A. C., Anderson, J. M., and Cantley, L. C. (1997) *Science 275*, 73−77.
13. Stricker, N. L., Christopherson, K. S., Yi, B. A., Schatz, P. J., Raab, R. W., Dawes, G., Bassett, D. J., Bredt, D. S., and Li, M. (1997) *Nat. Biotechnol. 15*, 336−342.
14. Murthy, K. K., Clark, K., Fortin, Y., Shen, S. H., and Banville, D. (1999) *J. Biol. Chem. 274*, 20679−20687.
15. Brenman, J. E., Chao, D. S., Gee, S. H., McGee, A. W., Craven, S. E., Santillano, D. R., Wu, Z., Huang, F., Xia, H., Peters, M. F., Froehner, S. C., and Bredt, D. S. (1996) *Cell 84*, 757−767.
16. Hillier, B. J., Christopherson, K. S., Prehoda, K. E., Bredt, D. S., and Lim, W. A. (1999) *Science 284*, 812−815.
17. Gee, S. H., Sekely, S. A., Lombardo, C., Kurakin, A., Froehner, S. C., and Kay, B. K. (1998) *J. Biol. Chem. 273*, 21980−21987.
18. Xu, X. Z., Choudhury, A., Li, X., and Montell, C. (1998) *J. Cell Biol. 142*, 545−555.
19. Cuppen, E., Gerrits, H., Pepers, B., Wieringa, B., and Hendriks, W. (1998) *Mol. Biol. Cell 9*, 671−683.
20. van Huizen, R., Miller, K., Chen, D. M., Li, Y., Lai, Z. C., Raab, R. W., Stark, W. S., Shortridge, R. D., and Li, M. (1998) *EMBO J. 17*, 2285−2297.
21. Banville, D., Ahmad, S., Stocco, R., and Shen, S. H. (1994) *J. Biol. Chem. 269*, 22320−22327.
22. Maekawa, K., Imagawa, N., Nagamatsu, M., and Harada, S. (1994) *FEBS Lett. 337*, 200−206.
23. Saras, J., Claesson, W. L., Heldin, C. H., and Gonez, L. J. (1994) *J. Biol. Chem. 269*, 24082−24089.
24. Lin, D., Gish, G. D., Songyang, Z., and Pawson, T. (1999) *J. Biol. Chem. 274*, 3726−3733.

25. Maekawa, K., Imagawa, N., Naito, A., Harada, S., Yoshie, O., and Takagi, S. (1999) *Biochem. J. 337*, 179−184.
26. Yanagisawa, J., Takahashi, M., Kanki, H., Yano, Y. H., Tazunoki, T., Sawa, E., Nishitoba, T., Kamishohara, M., Kobayashi, E., Kataoka, S., and Sato, T. (1997) *J. Biol. Chem. 272*, 8539−8545.
27. Saras, J., Engstrom, U., Gonez, L. J., and Heldin, C. H. (1997) *J. Biol. Chem. 272*, 20979−20981.
28. Schultz, J., Hoffmuller, U., Krause, G., Ashurst, J., Macias, M. J., Schmieder, P., Schneider, M. J., and Oschkinat, H. (1998) *Nat. Struct. Biol. 5*, 19−24.
29. Daniels, D. L., Cohen, A. R., Anderson, J. M., and Brunger, A. T. (1998) *Nat. Struct. Biol. 5*, 317−325.
30. Tochio, H., Zhang, Q., Mandal, P., Li, M., and Zhang, M. (1999) *Nat. Struct. Biol. 6*, 417−421.
31. Cabral, J. H., Petosa, C., Sutcliffe, M. J., Raza, S., Byron, O., Poy, F., Marfatia, S. M., Chishti, A. H., and Liddington, R. C. (1996) *Nature 382*, 649−652.
32. Muhlhahn, P., Zweckstetter, M., Georgescu, J., Ciosto, C., Renner, C., Lanzendorfer, M., Lang, K., Ambrosius, D., Baier, M., Kurth, R., and Holak, T. A. (1998) *Nat. Struct. Biol. 5*, 682−686.
33. Cho, K. O., Hunt, C. A., and Kennedy, M. B. (1992) *Neuron 9*, 929−942.
34. Schneider, S., Buchert, M., Georgiev, O., Catimel, B., Halford, M., Stacker, S. A., Baechi, T., Moelling, K., and Hovens, C. M. (1999) *Nat. Biotechnol. 17*, 170−175.
35. Ekiel, I., Banville, D., Shen, S. H., and Gehring, K. (1998) *Biochem. Cell Biol. 76*, 334−340.
36. Ekiel, I., Banville, D., Shen, S. H., Slon, U. J., Koshy, A., and Gehring, K. (1998) *J. Biomol. NMR 12*, 455−456.
37. Wishart, D. S., Bigam, C. G., Yao, J., Abildgaard, F., Dyson, H. J., Oldfield, E., Markley, J. L., and Sykes, B. D. (1995) *J. Biomol. NMR 6*, 135−140.
38. Delsuc, M. A. (1989) in Maximum enthropy and Bayesian methods (Skilling, J. Ed.), Kluwer Academic, Amsterdam.
39. Bartels, C., Xia, T.-H., Billeter, M., Guntert, P., and Wuthrich, K. (1995) *J. Biomol. NMR 5*, 1−10.
40. Altieri, A. S., Hinton, D. P., and Byrd, R. A. (1995) *J. Am. Chem. Soc. 117*, 7566−7567.
41. Stejskal, E. O., and Tanner, J. E. (1965) *J. Chem. Phys. 42*, 288−292.
42. Ekiel, I., Abrahamson, M., Fulton, D. B., Lindahl, P., Storer, A. C., Levadoux, W., Lafrance, M., Labelle, S., Pomerleau, Y., Groleau, D., LeSauteur, L., and Gehring, K. (1997) *J. Mol. Biol. 271*, 266−277.
43. Brunger, A. T., Adams, P. D., Clore, G. M., DeLano, W. L., Gros, P., Grosse-Kunstleve, R. W., Jiang, J.-S., Kuszewski, J., Nilges, M., Pannu, N. S., Read, R. J., Rice, L. M., Simonson, T., and Warren, G. L. (1998) *Acta Crystallogr., Ser. D 54*, 905−921.
44. Kuboniwa, H., Grzesiek, S., Delaglio, F., and Bax, A. (1994) *J. Biomol. NMR 4*, 871−878.
45. Gehring, K., and Ekiel, I. (1998) *J. Magn. Reson. 135*, 185−193.
46. Fesik, S. W., Eaton, H. L., Olejniczak, E. T., Zuiderweg, E. R. P., McIntosh, L. P., and Dahlquist, F. W. (1990) *J. Am. Chem. Soc. 112*, 886−888.
47. Bax, A., Clore, G. M., and Gronenborn, A. M. (1990) *J. Magn. Reson. 88*, 425−431.
48. Marion, D., Driscoll, P. C., Kay, L. E., Wingfield, P. T., Bax, A., Gronenborn, A. M., and Clore, G. M. (1989) *Biochemistry 28*, 6150−6156.
49. Grzesiek, S., Kuboniwa, H., Hinck, A., and Bax, A. (1995) *J. Am. Chem. Soc. 117*, 5312−5315.
50. Wang, A. C., and Bax, A. (1996) *J. Am. Chem. Soc. 118*, 2483−2494.
51. Archer, S. J., Ikura, M., Torchia, D. A., and Bax, A. (1991) *J. Magn. Reson. 95*, 636−641.
52. Szyperski, T., Neri, D., Leiting, B., Otting, G., and Wuthrich, K. (1992) *J. Biomol. NMR 2*, 323−334.
53. Corpet, F., Gouzy, J., and Kahn, D. (1999) *Nucleic Acids Res. 27*, 263−267.
54. Murthy, K. K., Ekiel, I., Shen, S. H., and Banville, D. (1999) *BioTechniques 26*, 142−149.
55. Kraulis, P. J. (1991) *J. Appl. Crystallogr. 24*, 946−950.
56. Nicholls, A., Sharp, K. A., and Honig, B. (1991) *Proteins 11*, 281−296.
57. Farmer, B., II, Constantine, K. L., Goldfarb, V., Friedrichs, M. S., Wittekind, M., Yanchunas, J. J., Robertson, J. G., and Mueller, L. (1996) *Nat. Struct. Biol. 3*, 995−997.

BI991913C